Multiobjective Optimization of SMB and Varicol Process for Chiral Separation

Ziyang Zhang, K. Hidajat, and Ajay K. Ray
Dept. of Chemical and Environmental Engineering, National University of Singapore, Singapore 119260

M. Morbidelli
Laboratorium fuer Technische Chemie, ETH-Hoenggerberg / HCI, CH-8093 Zurich, Switzerland

The multiobjective optimization of continuous countercurrent chromatography separation units, such as simulated moving bed (SMB) and Varicol, is considered. The Varicol system is based on a nonsynchronous shift of the inlet and outlet ports instead of the synchronous one used in the SMB technology. The optimization problem is complicated by the relative large number of decision variables, including continuous variables, such as flow rates and lengths, as well as discontinuous ones, such as column number and configuration. It is also important to reformulate the optimization problem as multiobjective, since the factors affecting the cost of a given separation process are multiple and often in conflict with each other. A typical example is simultaneous maximization of the productivity of the process and the purity of the corresponding products. A new optimization procedure based on a genetic algorithm allows handling these complex optimization problems. An existing literature chiral separation model was used to illustrate the potential of this optimization procedure. This work also offered a unique opportunity to compare the optimal separation performance achievable with the SMB and Varicol technologies.

Introduction

Process industries aim at maximizing their production capacities while simultaneously maintaining or improving product quality. Usually, a trade-off exists between these two requirements. This is particularly true in chiral separation using simulated moving-bed (SMB) systems (cf Strube et al., 1999; Juza et al., 2000; Rekoske, 2001) where purities of the products are crucial and have to satisfy relatively narrow specifications. Thus, the design and operation of SMBs (Charton and Nicoud, 1995) require optimization using multiple objective functions and constraints, which are often in conflict (Bhaskar et al., 2000a).

Several studies on the optimization of simulated moving-bed systems have been reported in the open literature (cf. Storti et al., 1988, 1995; Dunnebier and Klatt, 1999; Karlsson et al., 1999; Wu et al., 1999). These studies involve single (scalar) objective functions, which can include several objectives with weightage factors. This parametric approach is not efficient and also has the drawback that it could lose certain optimal solutions when the nonconvexity of the objective function gives rise to a duality gap, something that is very difficult to check out for complex, real-life problems. The use of multiobjective optimization with objective functions, which are vectors, provides a much better picture of the process and allows for more educated final decisions on the optimal operating point.

It is worth noting that single- and multiple-objective function optimization problems are conceptually different. In multiple-objective function optimization, there may not be a best solution (global optimum) with respect to all objectives. Instead, there *could* be an entire set of optimal solutions that are *equally* good. These solutions are known as Pareto-optimal (or nondominated) solutions. A Pareto set is defined such that when we go from any one point to another, at least one objective function improves and at least one other worsens. Thus, one cannot say that any one of these points is superior (or dominant) to any other, and, therefore, any one of the nondominated solutions in the Pareto set is an acceptable solution. The choice of one solution over the other requires

Correspondence concerning this article should be addressed to A. K. Ray.

additional knowledge of the problem, and often, this knowledge is intuitive and nonquantifiable. The Pareto set is very useful, however, since it narrows the choices and helps to guide a decision maker in selecting a desired operating point (called the preferred solution) from among the (restricted) set of Pareto-optimal points.

Multiobjective optimization has been an object of interest to engineers for a long time. But very few studies on multiobjective optimization have been reported in the mainstream chemical engineering literature, which recently has been reviewed by Bhaskar et al. (2000a). In that article, it was mentioned that an important process like the operation of SMB would be a suitable choice to explicate the importance of the idea of multiobjective optimization in chemical engineering. It is emphasized here that the work described herein is the *first* comprehensive multiobjective optimization study that has been made in this area.

SMB has been used in the petrochemical, sugar, and fine chemical industry for decades, due mostly to its separating power. Since the 1990s, SMB has drawn more and more attention for enantioseparation among drug producers, due to recent developments in chiral stationary phases (CSPs) and nonlinear chromatographic theory (Storti et al., 1993; Mazzotti et al., 1994, 1996, 1997; Migliorini et al., 1999), as well as a stringent drug administration policy. Even though the separating power of SMB is widely acknowledged, researchers are still trying to improve the performance of the SMB process to decrease the operating cost.

SMB is a practical implementation of true moving bed (TMB), where the problems caused by solid movement in the latter are avoided (Ruthven and Ching, 1989). In TMB, by properly arranging the relative flow rates between the fluid and solid phases in each of the four sections, each of which has its own specific separation task, weak and strongly adsorbed products can be separated and withdrawn from the raffinate port and extract port, respectively. In an equivalent SMB system, a fixed bed is used, and the movement of the solid is simulated by successive switching of the feed and product positions at timed intervals. The solid phase velocity can be defined as the ratio of the column length and the switching time. One obvious shortcoming of the SMB operating mode is that the velocity of the solid is constant in all sections, as constant values of both switching time and length are used. Recently, Ludemann-Hobourger et al. (2000) developed a novel process, Varicol, which is based on a *nonsynchronous* switch of the inlet and outlet ports. For illustrative purposes, they considered chiral (enantio) separation of 1,2,3,4-tetrahydro-1-naphthol racemate, using 20 μm of Chiralpak AD20 as the CSP and *n*-heptane, 2-propanol, and trifluroacetic acid as the eluent. They showed both experimentally and numerically that Varicol is indeed superior to SMB in terms of product purity and productivity. They found that similar purities could be achieved by a 5-column Varicol compared to a 6-column SMB process for the same productivity. They reported an 18.5% improvement in productivity for a 5-column Varicol system at almost the same eluent flow rate and product purity over a 6-column SMB process. However, this comparison was not definitive because no systematic optimization of the column configuration or operating conditions in the Varicol process was attempted.

In this work, a comprehensive optimization study of SMB and Varicol processes is reported using a state-of-the-art robust optimization technique, that is, a genetic algorithm (GA). GA is a nontraditional search and optimization method (Holland, 1975; Goldberg, 1989; Deb, 1995) that has become quite popular in engineering optimization. It mimics the principles of genetics and the Darwinian principle of natural selection (that is, survival of the fittest). The same chiral separation system reported by Ludemann-Hombourger et al. (2000) is considered to be an illustrative example. The optimization study is aimed either at improving the separation quality (product purities) with the same capital cost (fixed number and size of columns) and productivity (feed flow rate), or at reduced capital cost and/or eluent consumption and/or increased productivity for the same product purity requirements. Furthermore, by comparing the performance of the Varicol process with an equivalent SMB process, this work tries to determine to what extent operation of a SMB system can be improved by applying nonsynchronous switching with varying zone lengths.

The optimization method used in this work is very general, and can easily be applied to almost any other applications. In fact, in this article we *illustrate* the procedure to be used, and present solutions of a few relatively *simple* optimization problems with one or two objective functions. A whole variety of other problems can, indeed, be formulated and solved, depending upon one's interest.

In the past, multiobjective optimization problems were usually solved using a single *scalar* objective function, which was a weighted-average of several objectives ("scalarization" of the vector objective function). This process allows a simpler algorithm to be used, but unfortunately, the solution obtained depends largely on the values assigned to the weighting factors used, which is done quite arbitrarily. An even more important disadvantage of the scalarization of the several objectives is that the algorithm may miss some optimal solutions, which can never be found, regardless of the weighting factors chosen. This happens if the nonconvexity of the objective function gives rise to a duality gap (Deb, 1999; Fonseca and Fleming, 1998; Goicoechea et al., 1982). Several methods are available for solving multiobjective optimization problems, for example, the ϵ-constraint method (Chankong and Haimes, 1983; Hollingdale, 1978), goal attainment method (Fonseca and Fleming, 1998; Fleming, 1986), and the nondominated sorting genetic algorithm (NSGA) (Goldberg, 1989; Srinivas and Deb, 1995; Mitra et al., 1998; Deb, 1999). In this study we use NSGA to obtain the Pareto set. This technique offers several advantages (Deb, 1999, 2001), as for example, (1) its efficiency is relatively insensitive to the shape of the Pareto optimal front, (2) problems with uncertainties, stochasticities, and with discrete search spaces can be handled efficiently, (3) the "spread" of the Pareto set obtained is excellent (in contrast, the efficiency of other optimization methods decides the spread of the solutions obtained), and (4) it involves a single application to obtain the entire Pareto set (in contrast to other methods, such as the ϵ-constraint method, which needs to be applied several times over).

Indeed, NSGA has been applied recently to optimize several processes of industrial importance in chemical engineering, including an industrial nylon-6 semibatch reactor (Mitra

et al., 1998), a wiped-film polyester reactor (Bhaskar et al., 2000b, 2001), PMMA film reactor (Zhou et al., 2000), a steam reformer (Rajesh et al., 2000), beer dialysis (Yuen et al., 2000), cyclone separators (Ravi et al., 2000), hydrogen plant (Rajesh et al., 2001), and MTBE synthesis in SMBR (Zhang et al., 2002).

Simulated Moving-Bed System and Varicol Process

Figure 1a shows a 6-column SMB and the principle of its operation. It consists of columns of uniform cross section, each of length L and packed with an adsorbent. The columns are connected in series in a circular array. Two incoming fluid streams (Feed and Eluent) and two outgoing fluid streams (Extract and Raffinate) divide the system into four sections (I to IV), with 1, 2, 2, and 1 columns in each section, respectively, corresponding to the column configuration 1/2/2/1. Parameters Q_1, Q_2, Q_3, Q_4 are the fluid flow rates in sections I, II, III, and IV, respectively, while F and E are inlet flow rates of feed and eluent, respectively, and Ra and Ex are the outlet flow rates of raffinate and extract. However, only four of these eight flow rates are independent, as the remaining four are determined from the mass balance at points A, B, C and D (see Figure 1a). In particular, by fixing Q_1, Q_2, E, and F, all the other flow rates can be calculated using the following relations

$$\text{Point D:} \quad Ex = Q_1 - Q_2 \tag{1}$$

$$\text{Point A:} \quad Q_3 = Q_2 + F \tag{2}$$

$$\text{Point C:} \quad Q_4 = Q_1 - E \tag{3}$$

$$\text{Point B:} \quad Ra = Q_3 - Q_4 \tag{4}$$

Simulation of the countercurrent movement of the solid and the fluid is achieved by advancing the inlet and withdrawal ports, column by column, in the same direction as the fluid flow, at a predetermined switching time, t_s. Switching time and column configuration (the number of columns in each section) in SMB processes are usually decided *a priori* and remain constant during the entire operation.

In contrast to SMB, the Varicol process is based on the nonsimultaneous and unequal shift of the inlet/outlet ports. The concept and the principle of operation of the Varicol process, together with the equivalent SMB process, are illustrated in Figure 1b for one switching period. The switching

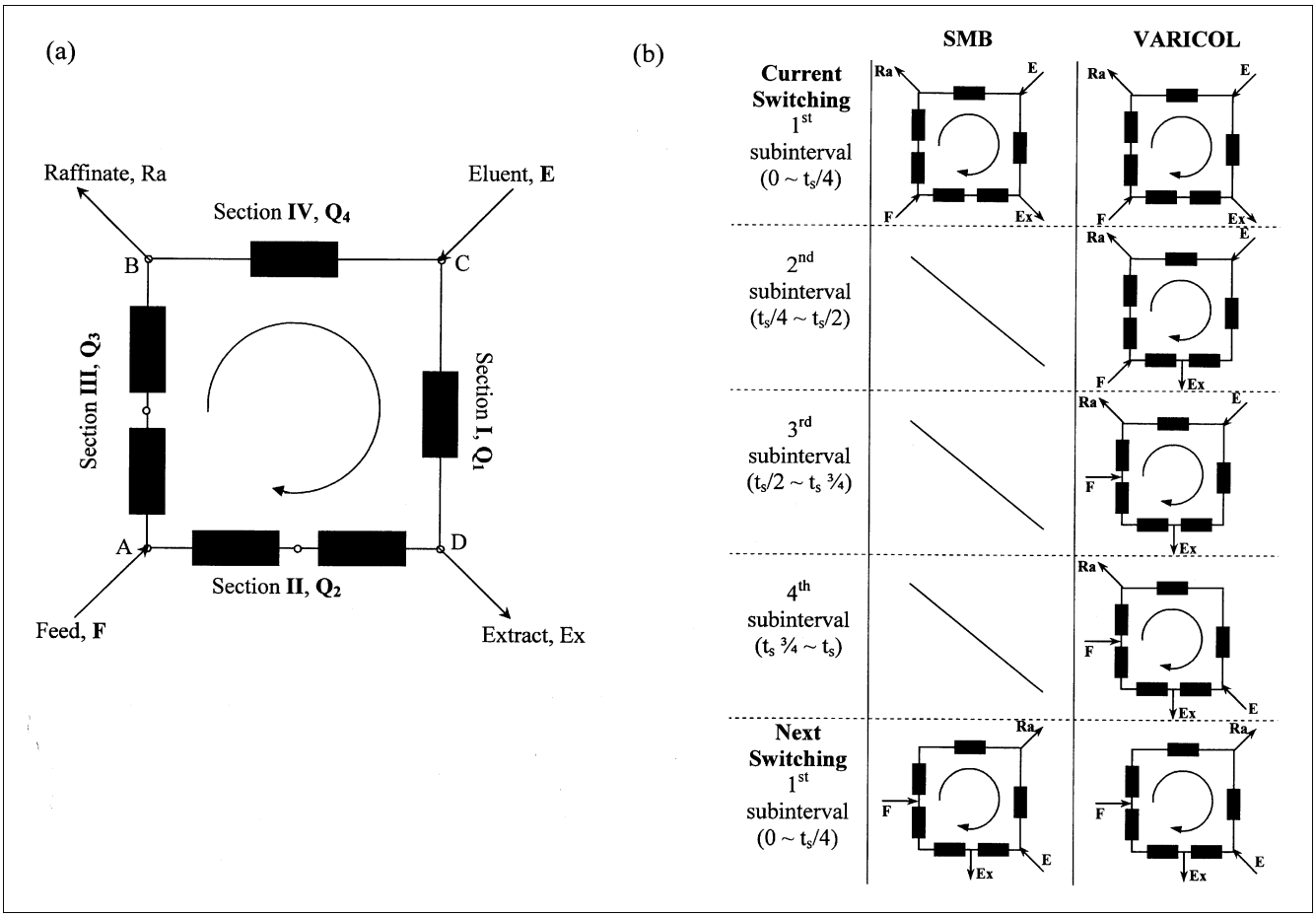

Figure 1. (a) SMB system with 6 columns. (b) Principle of operation of SMB and 4-subinterval Varicol systems (port switching schedule).

time, t_s, which is related directly to the solid flow rate in SMB, is also a key parameter in the Varicol process, although the relationship is not straightforward. In the Varicol operation, a nonsynchronous shift of the inlet and outlet ports, is usually employed within a switching period, which is again kept constant in time. This is shown as an illustrative example in Figure 1b for a 4-subinterval Varicol process. Within one (global) switching period, t_s, the column configuration changes from 1/2/2/1 ($0 \sim t_s/4$) to 2/1/2/1 ($t_s/4 \sim t_s/2$) by shifting the extract port by one column forward, then to 2/2/1/1 ($t_s/2 \sim t_s 3/4$) by shifting the feed port one column forward, then to 1/2/1/2 ($t_s 3/4 \sim t_s$) by shifting the eluent port one column forward, and finally returns to the original configuration of 1/2/2/1 by shifting the raffinate port one column forward. As a result, due to local switching during one global switching period, there are four different column configurations for the four subintervals in the 4-subinterval Varicol process. The number of columns in each zone varies with time within a global switching period, but the number of columns in each zone returns to the starting value at the end of the global switching period. In terms of the average number of columns per zone, this corresponds to the 1.5/1.75/1.5/1.25 configuration. Note that the average number for any particular zone is obtained as follows: for zone I, 1.5 is obtained from $(1+2+2+1)/4$, where the numbers in the parentheses are the number of columns in zone I in the 4-subintervals.

Therefore, the locations of the input/output ports in Varicol processes are quite different from those in SMB processes. Note that in principle it is possible that a port can shift more than once during one global switching period, either forward or even in the backward direction. As a result, Varicol processes can have several column configurations, which provide more flexibility compared to SMB processes. SMB processes can be regarded as a special case of the more flexible Varicol processes. It is remarkable that the Varicol process does not add any additional fixed cost.

Mathematical Model

In the open literature, the only reported results on the Varicol process are those of Ludemann-Hombourger et al. (2000) for the enantioseparation of 1,2,3,4-tetrahydro-1-naphthol, using the 20-μm Chiralpak AD as the CSP. They reported experimental results of both SMB and Varicol for this chiral separation, and also developed a model, which they showed could satisfactorily predict experimental results. In this article, we have adopted the same model for the SMB and the Varicol processes as that developed by Ludemann-Hombourger et al. (2000), which is based on the mixing cells in a series model (Charton and Nicoud, 1995). For SMB, during the Nth switching period, the mass-balance equation for component i in mixing cell k is given by

$$C_{i,N}^{(k-1)} = C_{i,N}^{(k)} + \left[\frac{t_0(\phi)}{J}\right]\frac{dC_{i,N}^{(k)}}{dt} + \left[\frac{1-\epsilon}{\epsilon}\right]\left[\frac{t_0(\phi)}{J}\right]\frac{d\overline{C}_{i,N}^{(k)}}{dt} \qquad 0 \le t \le t_s \quad (5)$$

whereas, for the Varicol process during the Mth subinterval of the Nth switching period, it is given by

$$C_{i,N,M}^{(k-1)} = C_{i,N,M}^{(k)} + \left[\frac{t_0(\phi)}{J}\right]\frac{dC_{i,N,M}^{(k)}}{dt} + \left[\frac{1-\epsilon}{\epsilon}\right]\left[\frac{t_0(\phi)}{J}\right] \times \frac{d\overline{C}_{i,N,M}^{(k)}}{dt} \qquad 0 \le t \le t_s/4; \qquad M = 1, 2, 3, \text{or } 4 \quad (6)$$

where J is the theoretical number of cells in the column, and $t_0(\phi)$ is the zero retention time of the column in section ϕ (I, II, III, or IV) and is given by

$$t_0(\phi) = \frac{\epsilon V_{\text{col}}}{Q_{\text{col}}(\phi)} \quad (7)$$

where $Q_{\text{col}}(\phi)$ is the volumetric flow rate in the column in section ϕ, and ϵ is the column external porosity, used as 0.4. Suitable boundary conditions must be used to properly simulate the process. The boundary conditions change with time due to the periodic operation scheme of the process according to the position of the various process streams. The concentration, $C_i^o(i_{\text{col}})$, can be easily calculated at the inlet of the column, i_{col}.

When the feed stream is connected to the inlet of a column, i_{col}, the concentration is given by

$$C_i^o(i_{\text{col}}) = \frac{[Q(i_{\text{col}}) - F]C_i^J(i_{\text{prev}}) + FC_{i,f}}{Q(i_{\text{col}})} \quad (8)$$

Table 1. Feed Composition, Adsorption Isotherm, and Column Hydrodynamics Used in the Optimization Studies

Feed Concentration	$C_{f,1} = C_{f,2} = 10$	g/L
Modified competitive Langmuir adsorption isotherms		g/L
	$\overline{C}_1 = 2.2C_1 + \dfrac{1.23C_1}{1 + 0.0647C_1 + 0.04655C_2}$	g/L
	$\overline{C}_2 = 2.63C_2 + \dfrac{1.35C_2}{1 + 0.0647C_1 + 0.04655C_2}$	
Pressure drop of each column (10 MM ID, 100 mm length)	$\Delta P/L = (632.3 \times 10^6) \cdot u$	SI units
Column efficiency (HETP)	$H_1 = 8 \times 10^{-5} + 0.200 \cdot u$	SI units
	$H_2 = 8 \times 10^{-5} + 0.244 \cdot u$	

Source: Ludemann-Hombourger et al. (2000).

When the eluent stream is connected to the inlet of a column, i_{col}, the concentration is given by

$$C_i^o(i_{col}) = \frac{[Q(i_{col}) - E]C_i^J(i_{prev})}{Q(i_{col})} \quad (9)$$

whereas in all other situations, we have

$$C_i^o(i_{col}) = C_i^J(i_{prev}) \quad (10)$$

with

$$\begin{cases} i_{prev} = i_{col} - 1 & \text{if } i_{col} > 1 \\ i_{prev} = N_{col} & \text{if } i_{col} = 1 \end{cases} \quad (11)$$

The outlet concentration of a component, i, at the exit of a column, i_{col}, is simply equal to the concentration, $C_i^J(i_{col})$. The extract and raffinate concentration can be obtained simply by using mass balances at points D and B, respectively (see Figure 1a).

Ludemann-Hombourger et al. (2000) also reported experimentally measured adsorption isotherms and column hydrodynamics (column efficiency and pressure drop as a function of the flow rates). They characterized the separation of the two enantiomers using an analytical column (4.6 mm ID, 250 mm long) packed with the stationary phase 20-μm Chiralpak AD. The adsorption isotherms and hydrodynamic equations, as well as the feed conditions used in their and our simulations, are summarized in Table 1.

The stiff initial-value ODEs were solved using the subroutine DIVPAG (which is based on Gear's method), in the IMSL library. Since periodic switching is imposed on the system, the separators work under transient conditions. However, a cyclic (periodic) steady state with a period equal to the global switching time is eventually reached after several switches. For both SMB and Varicol processes, the periodic steady state was always reached after about 20 cycles around the unit, that is, a number of switches equal to twenty times the total number of columns in the unit.

Optimization of SMB and Varicol Processes

Case I. Single-objective optimization: Maximization of throughput

In order to test the optimization procedure based on GA, we first compare our results with those reported by Ludemann-Hombourger et al. (2000) (which were obtained by trial and error without following a systemic optimization procedure), by considering the following optimization problem:

$$\text{Max} \quad J = F[Q_2, F, t_s, \chi] \quad (12a)$$

$$\text{Subject to} \quad PurE = 95\% \pm 0.2\% \quad (12b)$$

$$PurR = 95\% \pm 0.2\% \quad (12c)$$

$$Q_1 = 27.09 \text{ mL/min}, \; E = 6.24 \text{ mL/min}, \; N_{col} = 5, \; L = 0.1 \text{ m} \quad (12d)$$

$$\text{Model Eqs. 1–11, Table 1.} \quad (12e)$$

The objective function chosen is the feed flow rate, F, subject to the target purities of both extract, $PurE$, and raffinate, $PurR$, streams of 95%. The objective function (Eq. 12a) was modified in order to incorporate the two equality constraints (Eqs. 12b and 12c) by introducing suitable penalty functions. In addition, since the optimization code developed was for minimization of the objective function, the modified objective function actually used is given by

$$\text{Min} \quad I = \frac{1}{1+J} + w\left[1 - \frac{PurE}{0.95}\right]^2 + W\left[1 - \frac{PurR}{0.95}\right]^2. \quad (13)$$

A large value, $w(\approx 5\times 10^4)$, was used to achieve $PurE$ and $PurR$ within $\pm 0.2\%$ of the desired purity of 95%.

Four decision variables were used for this optimization study, as indicated by Eq. 12: flow rate in section II, Q_2; feed flow rate, F; switching time, t_s; and column configuration, χ. In order to be able to compare our results with those of Ludemann-Hombourger et al. (2000), we determined the total number of columns, $N_{col} = 5$, and two of the flow rates,

Table 2. Optimization Problems Solved in this Study and Bounds of Decision Variables

Problem No.		Obj. Func.	Constraints	Decision Variables	Fixed Parameters
Case I	SMB Varicol	Max F	$PurE = x \pm d$ $PurR = x \pm d$ $x = 95\%$ $d = 0.2\%$	$1.5 < F < 2.2$ mL/min $21 < Q_2 < 21.7$ mL/min $0.8 < t_s < 0.85$ min χ [see Table 3]	$N_{col} = 5$ $Q_1 = 27.09$ mL/min $E = 6.24$ mL/min $L = 0.1$ m
Case II	SMB Varicol	Max $PurE$ Max $PurR$	$PurE \geq 90\%$ $PurR \geq 90\%$	$21 < Q_2 < 23$ mL/min $0.78 < t_s < 0.85$ min χ [see Table 3]	$N_{col} = 5$ or 6, $L = 0.1$ m $Q_1 = 27.5$ mL/min $F = 1.62$ mL/min $E = 6.24$ mL/min
Case III	SMB Varicol	Max F Min E	$PurE = x \pm d$ $PurR = x \pm d$ $x = 90, 95, 99\%$ $d = 0.2\%$	$21 < Q_2 < 24$ mL/min $0.45 < F < 2.7$ mL/min $4.5 < E < 7.0$ mL/min $0.72 < t_s < 0.88$ min χ [see Table 3]	$N_{col} = 5$ $Q_1 = 27.5$ mL/min $L = 0.1$ m

Note that the bounds of the decision variables were restricted to even narrower ranges in some optimization refinement runs to achieve smooth (less scatter) distribution for the decision variable plots.

Table 3. Possible Column Configurations (distribution) for $N_{col} = 5$ and $N_{col} = 6$

χ	Column Configuration*	χ	Column Configuration
	$N_{col} = 5$		
A	2/1/1/1	*C*	1/1/2/1
B	1/2/1/1	*D*	1/1/1/2
	$N_{col} = 6$		
A	1/1/2/2	*F*	2/2/1/1
B	1/2/1/2	*G*	3/1/1/1
C	1/2/2/1	*H*	1/3/1/1
D	2/1/1/2	*I*	1/1/3/1
E	2/1/2/1	*J*	1/1/1/3

*Column distribution 2/1/1/1 implies two columns in section I and one column in sections II to IV.

$Q_1 = 27.09$ mL/min and $E = 6.24$ mL/min, to the optimum values obtained in their work. Since only four flow rates are free, while the other four are determined by Eqs. 1–4, the remaining two flow rates were used as decision variables: the feed flow rate, F, which is also the objective function, and Q_2. The third decision variable is the switching time, t_s, which clearly has a strong influence on the purity of the outlet streams. The bounds for t_s lie between the breakthrough times of the two components for a specific CSP. The optimization formulation and the bounds of the decision variables are summarized in the first row of Table 2. It is to be noted that a very narrow range is used for the bounds. This is required, as there exist narrow "windows" for the decision variables in order to get meaningful optimum solutions. Such boundaries can be estimated very conveniently using equilibrium theory and some preliminary sensitivity analysis of the model.

The fourth decision variable used is the column configuration (χ). For a fixed number of total columns ($N_{col} = 5$), there exist four possible column configurations, as reported in the first part of Table 3. In a SMB system, there is only one column configuration, which is fixed with time. However, in a Varicol process there are in principle infinite possible column configurations. In order to somehow restrict this variety, we consider here only 4-subinterval Varicol processes, assuming that in each subinterval the unit can take any one of the configurations possible for the SMB unit. For example, for a SMB process, $\chi = B$ indicates the column configuration 1/2/1/1, whereas, for a 4-subinterval Varicol process, $\chi = B$-*A*-*D*-*C* indicates that the sequence of column configurations *B*-*A*-*D*-*C* was used within the 4-subinterval global switching period. In terms of time-average column lengths, this corresponds to the configuration 1.25/1.25/1.25/1.25.

In Table 4 the optimum results obtained with GA when the feed flow rate was maximized for a SMB process are compared with the results of Ludemann-Hombourger et al. (2000) obtained by trial and error. It is seen that the GA optimization leads to a slightly larger feed flow rate, $F = 1.71$ mL/min, compared to 1.62 mL/min. The same optimum column configuration 1/2/1/1/ ($\chi = B$) was obtained, as were rather close values of the optimal Q_2 and t_s. For the equivalent 5-column Varicol process, the GA optimization leads to an optimum $F = 2.0$ mL/min, with an increase of 17% over the SMB process. When this result is compared with that of Ludemann-Hombourger et al., a 10% increase in the F value is found, as is a different optimum column configuration. In particular, the configuration $\chi = C$-*C*-*C*-*B* was found to be optimal, which, using the notation based on time-average column lengths, corresponds to 1/1.25/1.75/1 instead of 1/1.5/1.5/1. These comparisons, relative to single-objective optimization problems, show the reliability and efficiency of GA in finding optimal operating conditions, which compare well with previous results in the literature, and actually lead to slightly improved values of the objective functions. The unique capabilities and superiority of the GA will clearly appear later when we consider multiobjective optimization problems. We note in passing that it has been established that the Varicol process shows improvements over SMB operation.

Multiobjective Optimization of the SMB and Varicol Processes

The nondominated sorting genetic algorithm (NSGA) (Srinivas and Deb, 1995; Bhaskar et al., 2000) was used with the model described earlier to optimize the SMB and Varicol processes. NSGA generates a set of solutions that are nondominating over each other, and constitute multiobjective Pareto optimal solutions representing optimal operating conditions for the SMB and Varicol processes. We emphasize that there is no end to the variety of multiobjective optimization problems that can be formulated and studied, and we present a few examples here, to illustrate the concepts, techniques, and interpretation of results. We consider two multiobjective optimization cases in this study, which are typically encountered when considering separation processes of the

Table 4. Optimal Values for the Optimization Problem Described in Case I

	Ludemann-Hombourger et al. (2000)		This Work*	
	SMB	Varicol	SMB	Varicol
F, mL/min	1.62	1.82	*1.71*	*2.0*
Q_1, mL/min	27.09	27.04	27.09	27.09
Q_2, mL/min	21.31	21.27	*21.35*	*21.56*
E, mL/min	6.24	6.22	6.24	6.24
t_s, min	0.83	0.83	*0.82*	*0.81*
χ	*B*	1/1.5/1.5/1†	*B*	*C*-*C*-*C*-*B***
PurE	95%	95%	95%	95%
PurR	95%	95%	95%	95%

*Numbers in italic are optimum values obtained in this study from GA.
**Corresponding to 1/1.25/1.75/1.
†The average number of columns per zone described by Ludemann-Hombourger et al. (2000) as 1/1.5/1.5/1 could be achieved by many column distribution sequences such as *B*-*B*-*C*-*C*, *B*-*C*-*B*-*C*, *B*-*C*-*C*-*B*, *C*-*B*-*B*-*C*, *C*-*C*-*B*-*B*.

type under examination: the maximization of purity in both outlet streams and the maximization of throughput with minimization of eluent consumption.

Case II. Multiobjective optimization: Maximization of purity for the extract and raffinate streams

The first multiobjective optimization problem solved is the simultaneous maximization of the purity in the extract, *PurE*, and in the raffinate, *PurR*, stream for a given feed flow rate, F and eluent consumption, E. High product purity is typically an important requirement in drug manufacture. However, for a binary mixture with a low separation factor ($K_A/K_B < 1.2$), the high-purity requirement entails high cost and low throughput. In this case, the optimal design of the SMB and Varicol processes were performed for fixed capital and operation costs (number and length of column, that is, chiral stationary-phase volume, eluent flow rate, E, and overall system pressure drop), and throughput (feed flow rate, F). Having also fixed the flow rate in section I, Q_1 (which comes directly from fixing the maximum allowable pressure drop), the decision variables are Q_2, t_s, and χ. The optimization problem is represented mathematically as follows

$$\text{Max} \qquad J_1 = PurE\,[Q_2, t_s, \chi] \tag{14a}$$

$$\text{Max} \qquad J_2 = PurR\,[Q_2, t_s, \chi] \tag{14b}$$

$$\text{Subject to} \qquad PurE \geq 90\% \tag{14c}$$

$$PurR \geq 90\% \tag{14d}$$

$$F = 1.62 \text{ mL/min}, \; Q_1 = 27.5 \text{ mL/min}, \; E = 6.24 \text{ mL/min}$$

$$N_{col} = 5 \text{ or } 6, \; L = 0.1 \text{ m} \tag{14e}$$

$$\text{Model Eqs. 1–11, Table 1.} \tag{14f}$$

The choice of the two objective functions, J_1 and J_2, in Eqs. 14a and 14b enable the simultaneous maximization of the purity of the raffinate and extract streams. The inequality constraints (Eqs. 14c and 14d), which indicate the lowest acceptable purity values, were incorporated using penalty functions. The optimization problems (Eqs. 14a–14d) have then been written as

$$\text{Min} \qquad I_1 = \frac{1}{1+J_1} + w\sum_{i=1}^{2} f_i^2 \tag{15a}$$

$$\text{Min} \qquad I_2 = \frac{1}{1+J_2} + w\sum_{i=1}^{2} f_i^2 \tag{15b}$$

where

$$f_1 = [PurE - 0.90] - |[PurE - 0.90]| \tag{16a}$$

$$f_2 = [PurR - 0.90] - |[PurE - 0.90]|. \tag{16b}$$

In Eqs. 15a and 15b, the large numerical weighting factor on the operational constraints penalizes objectives, I_1 and I_2, in the event of constraint violation. The bounds of the decision variables are given in Table 2.

The results of the optimization run are shown in Figure 2, where the purity of the extract, *PurE*, is plotted as a function of the purity of the raffinate, *PurR*, for a 5-column and a 6-column SMB, and a 5-column Varicol process. The values

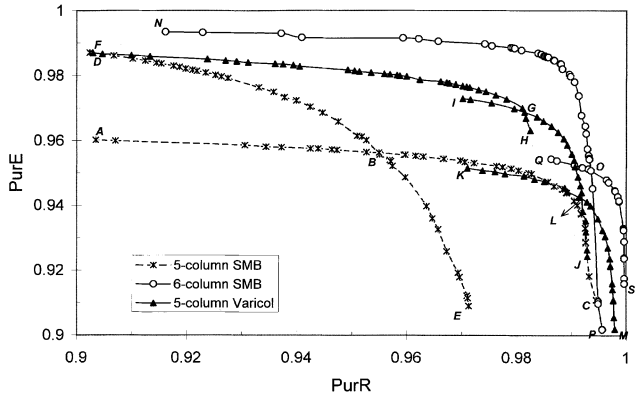

Figure 2. Pareto optimal solution for case II for SMB and Varicol systems.

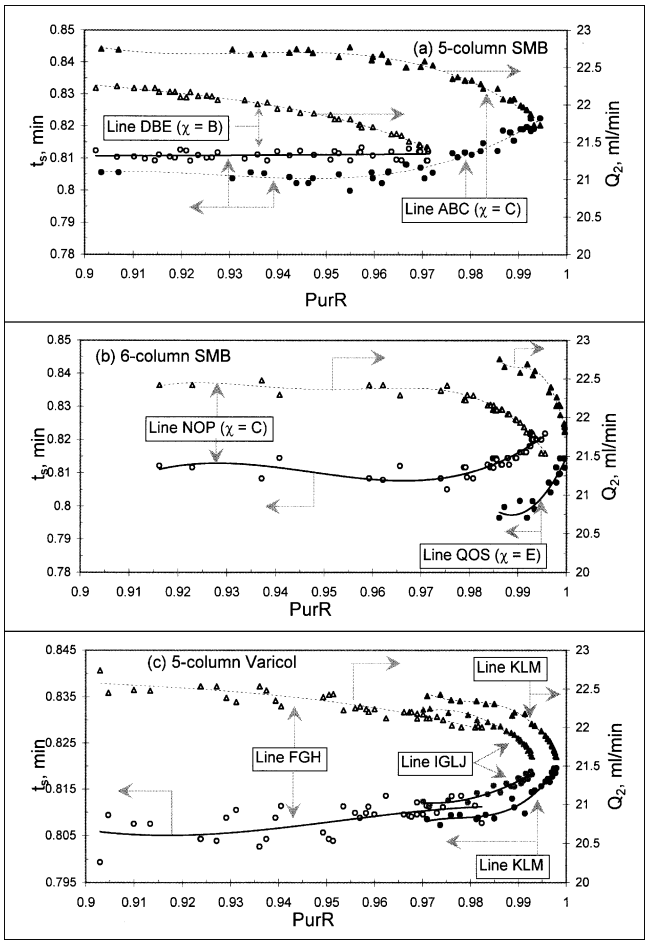

Figure 3. Decision variables (Q_2, t_s) corresponding to the points on Pareto sets in Figure 2.

Table 5. Optimum Column Configurations for the Paretos Shown in Figures 2 and 8

Figure No.	Process	Pareto Line	Column Configuration, χ
2	5-column SMB	*ABC*	*C*
		DBE	*B*
	6-column SMB	*NOP*	*C*
		QOS	*E*
	5-column Varicol	*FGH*	*C-C-B-B*
		IGLJ	*C-C-C-B*
		KLM	*C-C-C-A*
8	$Q_1 = 26$ mL/min (5-column Varicol)	*TU*	*C-C-B-B*
		UV	*C-C-C-B*
		VW	*C-C-C-A*
	$Q_1 = 29$ mL/min	*XY*	*C-C-B-B*
		YZ	*C-C-B-A*
		ZA	*C-C-C-A*

of *PurR* and *PurE* are plotted rather than those of I_1 and I_2, since the penalty functions have no contribution to the objective functions on attainment of convergence. Plotting the physical objectives directly rather than the actual objective function gives a better perspective when one is required to choose or discriminate among the various operating scenarios.

First let us consider the optimization of the 5-column SMB process. When the optimization run is carried out using the column configuration (χ) as a decision variable parameter, as stated in the optimization, formulation, Eqs. 14–16, and Table 2, line *DBC* is obtained. It can be easily observed that the points on line *DBC* do, indeed, constitute a Pareto set, that is, as we move from point *D* to point *C* along line *DBC*, *PurR* increases while *PurE* decreases. One cannot improve purity of one stream without sacrificing purity of the other stream, unless by violating the process constraints given by Eq. 14e. Each point (referred to as a chromosome) on the Pareto set is associated with a set of decision variables. Figure 3a is a plot of the decision variables (Q_2 and t_s) that correspond to each of the points on the Pareto set. Table 5 shows the corresponding optimal column configuration, χ. To obtain the operating conditions for a desired purity level, a designer has to read the values of the decision variables corresponding to the desired abscissa value from Figure 3a, and the corresponding optimum χ from Table 5. It can be seen that the Pareto *DBC* exhibits a discontinuity at the point *B*. This is due to the fact that the optimum column configuration changes, that is, it is found to be $\chi = B$ along branch *DB* and $\chi = C$ along *BC* (see Table 3). In order to confirm these results, we ran two additional optimization runs identical to those described by Eqs. 14–16 and Table 2, except fixing $\chi = B$ or *C* instead of allowing it to vary. Pareto lines *ABC* (when $\chi = C$) and *DBE* (when $\chi = B$) were obtained. The comparison with Pareto line *DBC* obtained earlier shows the flexibility and effectiveness of the optimization package (NSGA) in finding the Pareto optimal solution in a single run (given by line *DBC*) when the column configuration was left free as a decision variable.

Similarly, Pareto line *NOS* (Figure 2) was obtained for a 6-column SMB process when χ was allowed to vary according to values given in Table 3, while Pareto lines *NOP* and *QOS* were obtained when χ was fixed at *C* and *E* (see Table 5), respectively. The corresponding optimal values of decision variables Q_2 and t_s are shown in Figure 3b. When optimization for the 4-subinterval 5-column Varicol process was carried out with χ as a decision variable, Pareto line *FGLM* in Figure 2 and the optimal values of Q_2 and t_s shown in Figure 3c were obtained. Likewise, Pareto lines *FGH*, *IGLJ*, and *KLM* were obtained when the sequence for χ was fixed as *C-C-B-B*, *C-C-C-B*, and *C-C-C-A*, respectively, as reported in Table 5.

The following noteworthy conclusions can be drawn from the results shown in Figure 2. First, the Pareto optimal solutions obtained (line *DBC* for the 5-column SMB, line *NOS* for the 6-column SMB, and line *FGLM* for the 5-column Varicol) represent the maximum possible product purities of raffinate and extract streams for either the Varicol or the SMB process. The benefit of a multiobjective optimization is evident upon observing the wide choice of operating points available in the optimal Pareto set. If conventional techniques were used, we would have been able to predict only one point at a time on the optimal Pareto curves, by fixing either one of the purity values and maximizing the other.

Second, from Figure 2 we can see that for the same CSP volume (N_{col}, L), productivity (F), eluent flow rate (E), and maximum allowable pressure drop (Q_1), a 5-column, 4-subinterval Varicol system can attain higher purity levels compared to an equivalent 5-column SMB system, if the operating process parameters are properly chosen. It is found that the improvement is significant when high purities are requested for both products. For example, if the desired purity of raffinate stream, *PurR*, is set equal to 96%, then the maximum possible attainable extract purity, *PurE*, is 98% in a 5-column Varicol system compared to only about 95.6% in a 5-column SMB system. However, in the case where only one very high-purity product stream is required, the difference between Varicol and SMB system decreases. In the limit where a high purity level of one or the other stream is desired, the two extreme points (for example, points *D* and *F*) of the two Pareto lines (*DBC* and *FGLM*) may become very similar, although it has to be appreciated that even small differences at such very high purity values can be very significant.

Third, the maximum attainable purities in a 5-column Varicol system are less than those that can be obtained in a 6-column SMB. In other words, in this case, the increase in achievable product purities in a 6-column SMB system due to the increase of one column (which implies a 20% increase of stationary phase) outweighs the improvement attainable due to the increase in flexibility in a 5-column, 4-subinterval Varicol system, which, on the other hand, does not imply any additional cost.

In order to better appreciate the reliability of the optimization procedure, it is worth commenting on the results obtained using the simple findings of the equilibrium theory applied to countercurrent chromatography (Storti et al., 1995). These findings show that the unit behavior can be explained in terms of the flow-rate-ratio parameters relative to the four sections of the unit

$$m_j = \frac{Q_j t_s - V_{col}\epsilon}{V_{col}(1-\epsilon)}, \qquad j = 1 \sim 4 \tag{17}$$

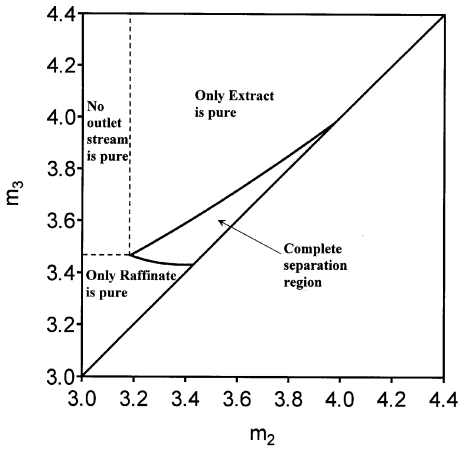

Figure 4. Complete separation region in the (m_3, m_2) plane for the binary separation in Table 1.

In particular, flow-rate-ratio parameter, m_1, has to be larger than a critical value in order to achieve complete regeneration of the solid phase from the strongly adsorbed (heavy) component, while m_4 has to be smaller than a critical value in order to achieve complete regeneration of the liquid phase from the weakly adsorbed (light) component. Once both such conditions are satisfied, it is possible to identify in the ($m_3 - m_2$) parameter plane a triangular region, which includes all pairs of values leading to a complete separation, that is, the two components are recovered pure in the extract and in the raffinate, respectively. This region, which depends only on the adsorption isotherms and the feed concentrations, has been calculated according to Gentilini et al. (1998) and is represented in Figure 4. In the upper right region, with respect to that of complete separation, a pure extract stream is obtained, while the raffinate is polluted. In the lower left region, only the raffinate and not the extract is obtained pure. Finally, it is worth mentioning that the distance from the diagonal of a point in the ($m_3 - m_2$) plane is directly proportional to productivity and inversely proportional to the desorbent requirement. Thus, the optimal operating point with respect to these two process performances, which also provides complete separation, is given by the vertex of the complete separation triangular region.

In order to interpret the results of the optimization, let us replot the optimal values of the decision variables in Figure 3 in terms of the four flow-rate-ratio parameters, m_j, as shown in Figures 5 to 7 for the 5-column SMB, the 6-column SMB, and the 5-column Varicol process, respectively. Starting with Figure 5, we see that all operating points on the Pareto line correspond to a substantially constant value of m_1, in agreement with the equilibrium theory, which predicts a constant lower bound for this parameter. We observe an increase in m_1 only for the points corresponding to the higher raffinate purity values. This is due to the necessity of improving the solid regeneration in section I in order to avoid having the heavier component enter section IV and then pollute the raffinate. The flow-rate ratio in section IV, m_4, follows similar behavior to m_1. This is again in agreement with the equilibrium theory, and it is also a consequence of the fact that E and Q_1 are fixed in this problem, thus, providing a fixed relation between m_1 and m_4. This justifies the increase in m_4 at large raffinate purity values, which on the other hand, affects negatively the purity of the extract in a region where this purity is expected to be low anyway. The values of m_2 and m_3 do not vary much, according to equilibrium theory, which would see them constant and corresponding to the vertex of the complete separation region. However, due to dispersion phenomena, the same change in m_2 and m_3 is observed, and actually they both tend to decrease, as moving along the Pareto line from points with high extract and low raffinate purities to points with low extract and high raffinate purities. This can be understood by noting that it corresponds in the (m_2 and m_3) plane in Figure 4 to a movement from the high extract purity to the high raffinate purity region. Another interesting observation is that when passing from the *ABC* branch of the Pareto line to the *DBE* branch, both m_2 and m_3 decrease. This is in agreement with the fact that in branch *ABC* the SMB configuration is 1/1/2/1 ($\chi = C$), while in the *DBE* branch it is 1/2/1/1 ($\chi = B$). This means that going from *ABC* to *DBE*, the job of section III (which is to adsorb the heavier component) becomes more difficult, since we have

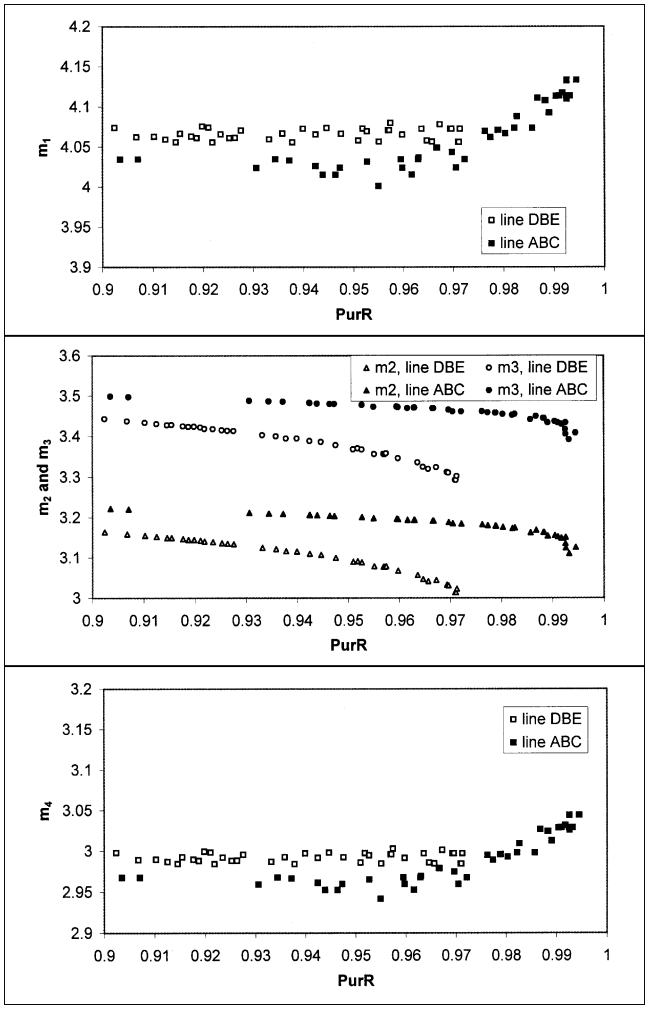

Figure 5. Flow-rate ratio parameter m_1 to m_4 corresponding to the points on the Pareto sets of 5-column SMB in Figure 2.

one column less and, thus, have to decrease m_3, while the job of section II (which is to desorb the weaker component) becomes easier, since we have one column more, and, therefore, we can operate with lower values of m_2. Similar behavior can be observed in Figures 6 and 7 for the 6-column SMB process and the 5-column Varicol process, respectively. The only additional comment required is that higher raffinate purities are achieved in these cases, and, therefore, the increase in m_1, and consequently in m_4, is more pronounced than in the case of a 5-column SMB.

The optimal column configurations obtained for the three processes reported in Table 5 can be rationalized by recalling that in countercurrent chromatography units, sections I and III are responsible for the purity of the raffinate, while sections II and IV control the purity of the extract. Thus, for the 5-column SMB we see that, as the raffinate purity increases, we go from branch *DBE* to branch *ABC*, which means from a 1/2/1/1/ to a 1/1/2/1 configuration, that is, the extra column moves from the second to the third section. For the 6-column SMB process, by increasing the raffinate purity, we go from branch *NOP* with configuration 1/2/2/1 to branch

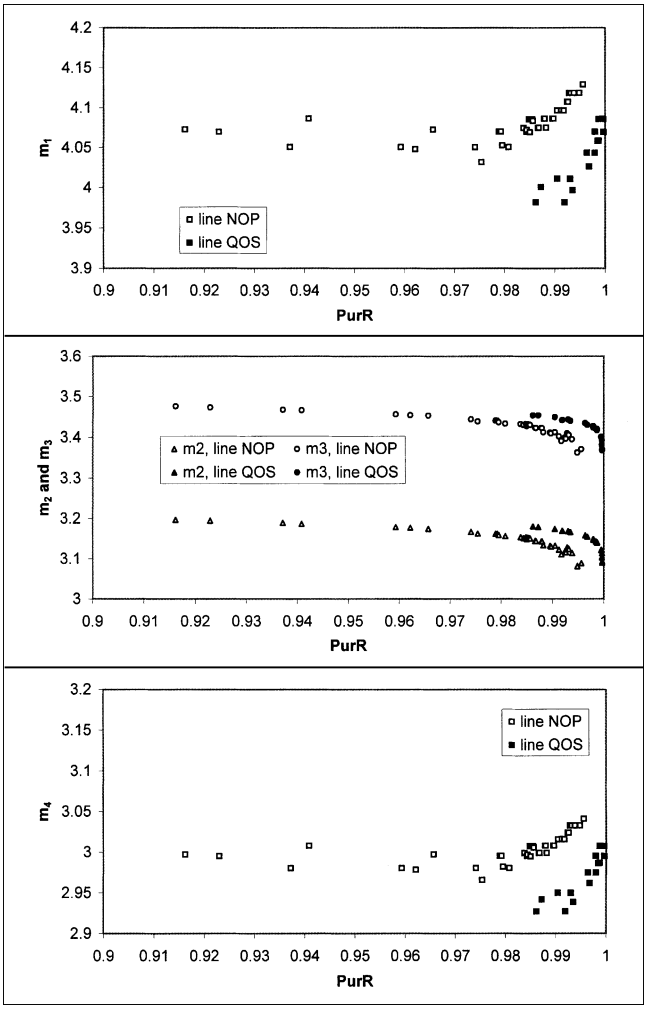

Figure 6. Flow-rate ratio parameter m_1 to m_4 corresponding to the points on the Pareto sets of 6-column SMB in Figure 2.

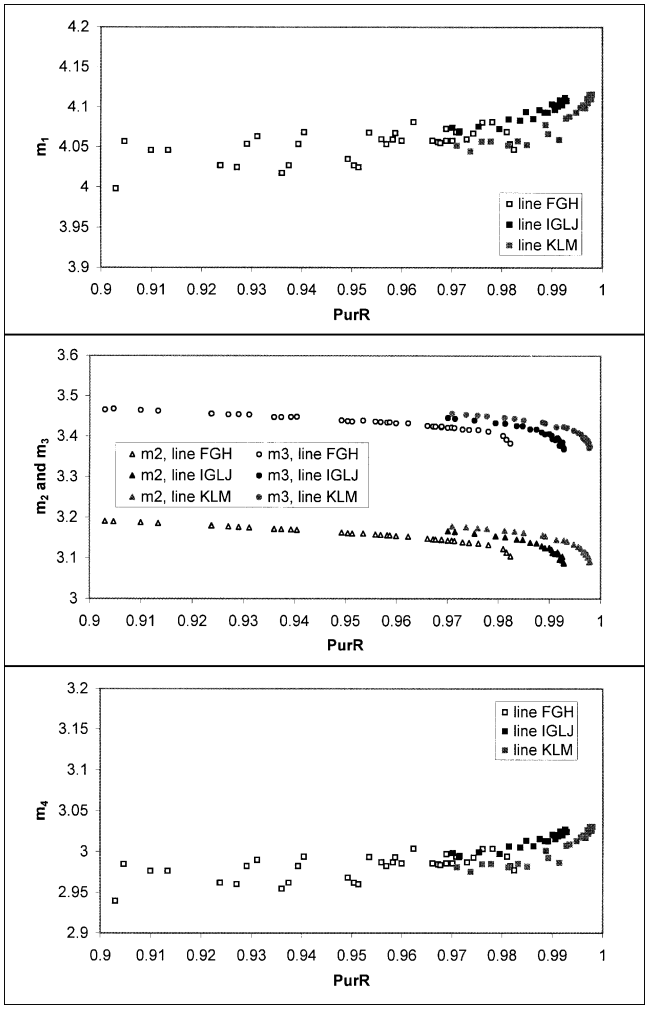

Figure 7. Flow-rate ratio parameter m_1 to m_4 corresponding to the points on the Pareto sets of 5-column Varicol in Figure 2.

QOS with configuration 2/1/2/1. In this case, since section III already has two columns, the second column in section II is moved to section I. This confirms that in the conditions of very high raffinate purity, it is section I that becomes critical, as indicated by the increase in m_1 observed in Figures 5 to 7. Finally, for the 5-column Varicol process, three branches appear in series corresponding to *C-C-B-B*, *C-C-C-B* and *C-C-C-A*, which in the alternative notation based on time-average column length corresponds to 1/1.5/1.5/1, 1/1.25/1.75/1, and 1.25/1/1.75/1, respectively. This shows again that in order to achieve higher raffinate purities sections III and I are reinforced at the expense of section II. Note that the flexibility of Varicol allows such a transition to be made more smoothly and the separation requirements to be followed more closely than does the SMB process. This justifies the improvement in its performance. It is worth observing that the preceding interpretation, which is based on the basic concepts of equilibrium theory, helps to rationalize the results of the optimization procedure, which when plotted in terms of the original variables (that is, Figure 3) indeed appear a bit confusing.

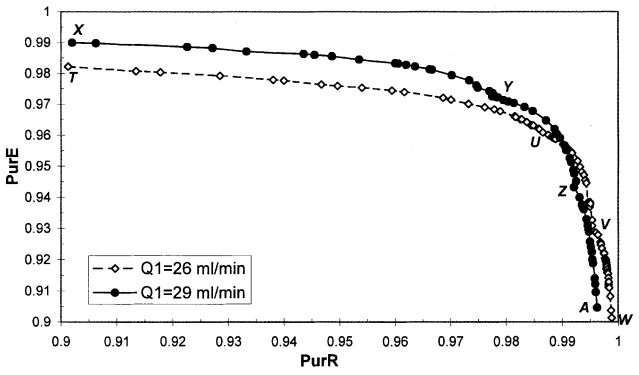

Figure 8. Effect of Q_1 for case II optimization in a 5-column Varicol system.

Effect of flow rate in section I, Q_1. Figure 8 illustrates the shift in the optimal Pareto set of the 5-column Varicol process when the flow rate in section I, Q_1, is changed with respect to the reference value $Q_1 = 27.5$ mL/min considered in the previous section. The corresponding distributions of optimal decision variables are shown in Figures 9 and 10 in terms of the flow-rate-ratio parameters, while the optimal column configurations are reported in Table 5.

These results are at first glance surprising, since an increase in the value of Q_1 would seem to imply better regeneration of section I, and, therefore, larger raffinate purities, which is the opposite of what is shown in Figure 8. These results can be interpreted by considering that, since in this problem the flow rates of feed and eluent are kept constant, all the internal flow rates in the unit increase as Q_1 is increased. However, in the previous section we have seen that the optimal values of m_2 and m_3 should remain substantially unchanged, and that the system, therefore, reduces the t_s values in contrast to the increase in Q_2 and Q_3. The problem is that this leads to smaller values of m_1 and m_4, too, and while the latter is beneficial for the extract purity, instead it has a negative effect for the raffinate purity. This can be seen in Figures 9 and 10, where by increasing Q_1 from 26 mL/min to 29 mL/min the largest observed change in the m values is that for m_1, which actually decreases from about 4.1 to about 4.0, thus, justifying the results in Figure 8, which show that at larger Q_1 values the unit achieves better performances when high extract purities are requested, but poorer performances when high raffinate purities are requested.

Note that this result is consistent with the sequence of optimal column configurations reported in Table 5. For $Q_1 = 26$ and 27.5 mL/min, this in fact changes from 1/1.5/1.5/1 to 1/1.25/1.75/1 to 1.25/1/1.75/1 as the required raffinate purity increases. On the other hand, for $Q_1 = 29$ mL/min, this goes from 1/1.5/1.5/1 to 1.25/1.25/1.5/1 to 1.25/1/1.75/1, which, in this case, indicates that section I becomes more critical, and, therefore, an extra column has to be transferred to section I at lower raffinate purities than in the previous cases at lower Q_1 values.

Case III. Multiobjective optimization: Maximization of throughput and minimization of eluent consumption

Another application situation of interest is one where the product purities are fixed, and the objectives for the optimal

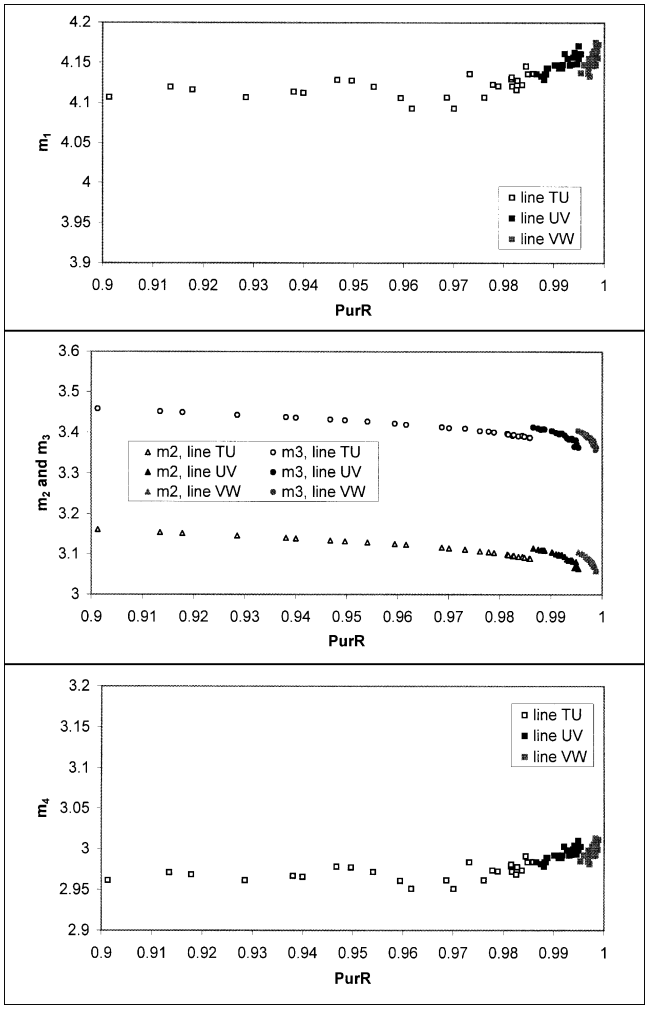

Figure 9. Flow-rate ratio parameters m_1 to m_4 corresponding to the points on the Pareto sets of 5-column Varicol in Figure 8 ($Q_1 = 26$ mL/min).

process operation are to reduce operating costs and increase production. Hence, in this case, for a fixed target product purity of both the extract and raffinate streams, we seek to determine the optimal process parameters for the 5-column SMB and Varicol systems, which maximize production using a minimum amount of eluent. The optimization problem is represented mathematically as follows

$$\text{Max} \qquad J_1 = F[Q_2, F, E, t_s, \chi] \tag{18a}$$

$$\text{Min} \qquad J_2 = E[Q_2, F, E, t_s, \chi] \tag{18b}$$

$$\text{Subject to} \qquad \text{PurE} = x \pm 0.002,\ x = 0.90, 0.95, 0.99 \tag{18c}$$

$$\text{PurR} = x \pm 0.002,\ x = 0.90, 0.95, 0.99 \tag{18d}$$

$$Q_1 = 27.5 \text{ mL/min},\ N_{\text{col}} = 5,\ L = 0.1 \text{ m} \tag{18e}$$

$$\text{Model Eqs. 1–11, Table 1.} \tag{18f}$$

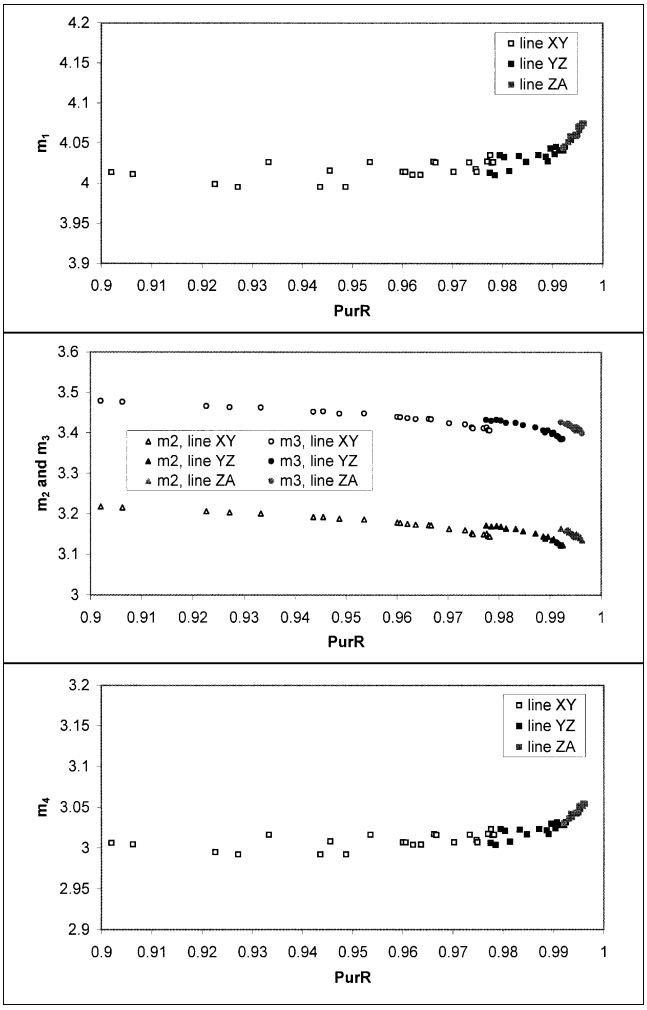

Figure 10. Flow-rate ratio parameters m_1 to m_4 corresponding to the points on the Pareto sets of 5-column Varicol in Figure 8 ($Q_1 = 29$ mL/min).

The choice of the two objective functions, J_1 and J_2, in Eqs. 18a and 18b allows the simultaneous maximization of production and minimization of eluent consumption for fixed target product purity (Eqs. 18c and 18d). The inequality constraints were incorporated using penalty functions in the objective functions as follows

$$\text{Min} \qquad I_1 = \frac{1}{1+J_1} + w\left[\frac{PurE - x}{x}\right]^2 + w\left[\frac{PurR - x}{x}\right]^2 \tag{19a}$$

$$\text{Min} \qquad I_2 = J_2 + w\left[\frac{PurE - x}{x}\right]^2 + w\left[\frac{PurR - x}{x}\right]^2 \tag{19b}$$

where $x = 0.90$, 0.95 and 0.99.

As in case II, Q_1, the column flow rate in section I was fixed at 27.5 mL/min to keep the maximum system pressure drop constant, and the total CSP used was also set by fixing $N_{col} = 5$ and $L = 0.1$ m. The details of the optimization formulation are reported in Table 2, together with the bounds used for the decision variables. Note that the two variables (F and E) appear in the objective functions as well as in the decision variables. The optimal Pareto solutions (E vs. F) and the values of the related decision variables (in terms of the m parameters) are shown in Figures 11 to 13 for the desired purity requirement of 90%, 95% and 99%, respectively, for both the extract and raffinate streams. The corresponding optimal column configurations are reported in Table 6. The Pareto lines shown in Figures 11 to 13 indicate, as expected, that as the treated feed flow rate increases, the minimum required eluent also increases. On the other hand, it is seen that the values of m_2 and m_3 obtained in both cases change very little as the feed flow rate increases. This is consistent with the equilibrium theory result discussed in the context of Figure 4, which indicates that the optimal operating point (the vertex of the triangle) is independent of the feed and eluent flow rates. It may be seen, however, that as

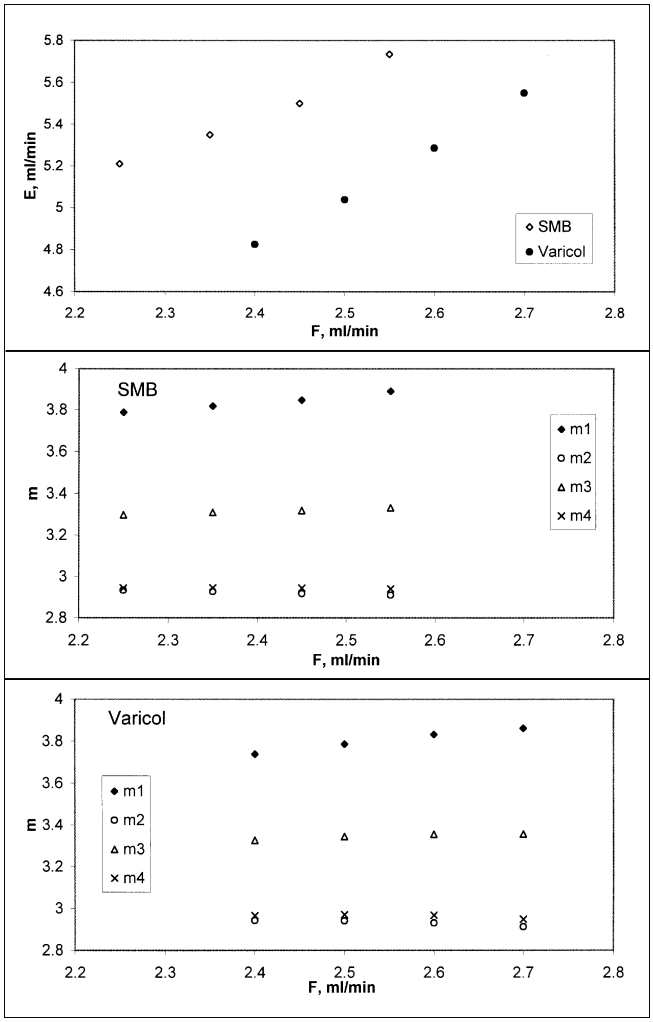

Figure 11. Pareto sets and corresponding values of flow-rate ratio parameter m_1 to m_4 for case III with 90% purity requirement for both extract and raffinate.

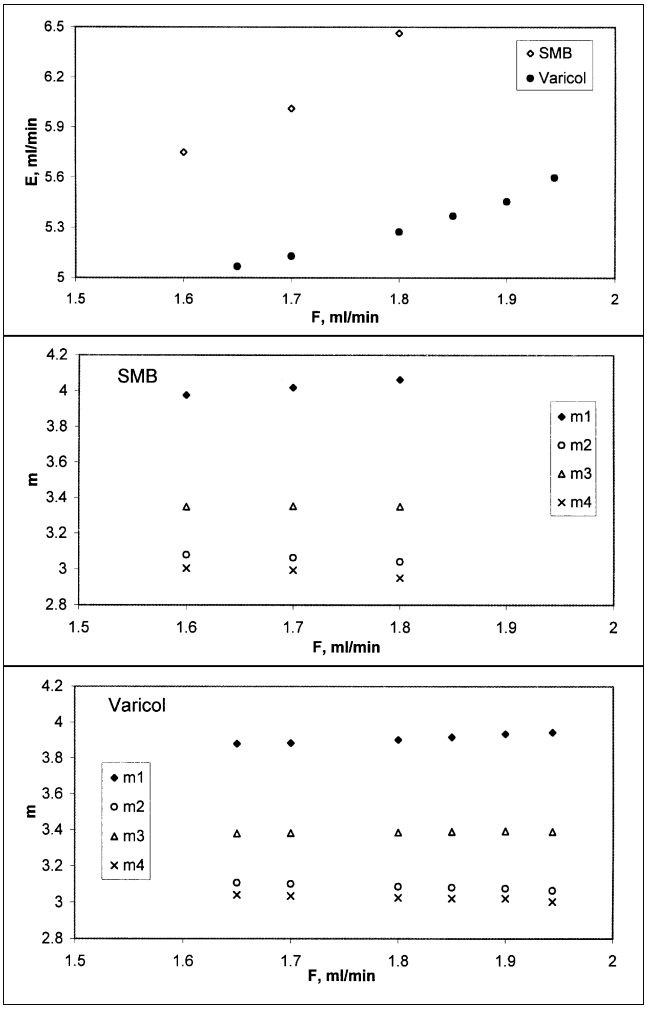

Figure 12. Pareto sets and corresponding values of flow-rate ratio parameter m_1 to m_4 for case III with 95% purity requirement for both extract and raffinate.

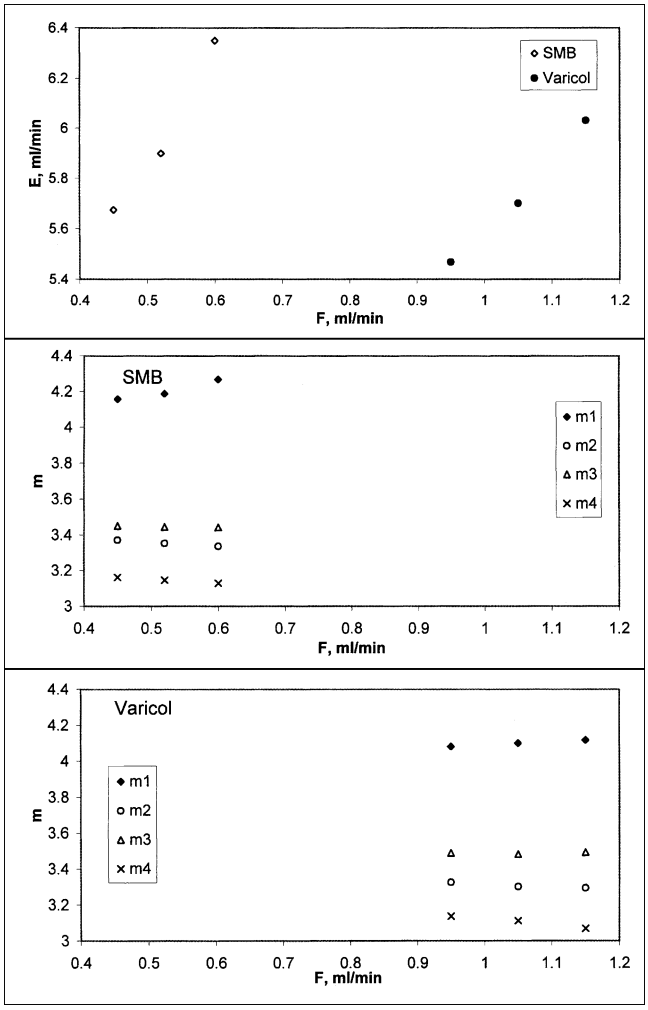

Figure 13. Pareto sets and corresponding values of flow-rate ratio parameter m_1 to m_4 for case III with 99% purity requirement for both extract and raffinate.

the required purities increase, that is, going from Figure 11 to Figure 13, the values of m_2 increase, as, to a lesser extent, do the values of m_3. This can be understood by considering that, since more stringent purity specifications have to be satisfied, the operating point leaves the vertex and enters the complete separation region more deeply, as shown in Figure 4, in order to balance the effect of the dissipative processes, and this corresponds to the changes in m_2 and m_3 just mentioned. On the other hand, the difference $(m_3 - m_2)$ decreases significantly in agreement with the decrease in the feed flow rate that can be treated as the purity specifications increase from Figure 11 to Figure 13. The values of m_1 that marginally increase with increasing F are consistent with the need to improve the regeneration conditions in section I due to the increased flow rates to be treated. This indicates that section I is critical in controlling the purity in the raffinate as production increases. We need to better control the regeneration of the solid from the heavy component in section I. This conclusion is confirmed by the fact that such changes become more pronounced as the purity specifications become stricter, that is, going from Figure 11 to Figure 13. On the other hand, m_4 undergoes smaller changes, indicating that section IV is much less critical in achieving the desired separation performance in the particular case under examination. As a consequence of the fact that the performance of the separation (that is, the flow-rate-ratio parameter values) re-

Table 6. Optimum Column Configurations for the Paretos Shown in Figures 11 to 13 for 5-Column SMB and Varicol Systems

Figure No.	Desired Product Purity	Process	χ
11	0.90	SMB	*B*
		Varicol	*D-C-C-B*
12	0.95	SMB	*B*
		Varicol	*D-C-C-B*
13	0.99	SMB	*B*
		Varicol	*D-C-C-B**

*χ for Varicol in Figure 13 for $F = 1.15$ mL/min is *C-C-C-B*.

mains substantially constant for all the operating points along the Pareto line, the optimal column configuration also remains the same both for the SMB and the Varicol processes, and equal to 1/2/1/1 and 1/1.25/1.50/1.25, respectively, as reported in Table 6. This result again shows the flexibility of Varicol in distributing the columns in the various sections of the unit in order to improve the separation performance.

To summarize, the following conclusions can be drawn. For fixed purity specifications, both the SMB and the Varicol processes must increase eluent consumption in order to increase the feed flow rate. Second, under the same conditions, the Varicol process consumes less eluent, E, than an equivalent SMB process for the same feed flow rate, F; or for the same eluent consumption, E, the Varicol process can treat more feed, F. Thus, it is confirmed and quantified that the flexibility due to the nonsynchronous shift of the input/output ports in a Varicol process allows the same desired target purity to be achieved with less eluent and/or allows more feed to be treated. However, the degree of improvement depends on the purity specifications. The larger the desired purity requirement, the larger the improvement achieved by a Varicol over a SMB system. For example, at $E = 5.6$ mL/min, the improvement in productivity, F, of a Varicol system over an equivalent SMB process is 10%, 25%, and 127% for the desired target purity requirement of both the extract and raffinate streams of 90%, 95%, and 99%, respectively. Finally, the optimum number of columns in each section (column configuration, χ) obtained is the same irrespective of the desired target purity requirement for both SMB and Varicol processes (see Table 6), while the feed flow rate that can be treated decreases as the purity specifications become more stringent.

Effect of Number of Subintervals and Columns in the Varicol Process. So far we have considered only the 4-subinterval, 5-column Varicol process. It can be easily seen that when the number of subintervals and columns is increased in a Varicol system, its flexibility increases, and this leads to better separation performances. In this section, we compare the optimum eluent flow rate required for a 5-subinterval, 5-column Varicol process, a 4-subinterval, 6-column Varicol process, and a 4-subinterval, 5-column Varicol process. The formulation and results of the optimization problem are summarized in Table 7. The 5-subinterval Varicol process is the same as that of a 4-subinterval Varicol process, except that the input/output ports are allowed to shift every 1/fifth instead of every quarter of the global switching period, t_s. In the 6-column Varicol configuration, we have added one column, but of reduced column length, in order to keep the total volume of the solid (V_{CSP}) equal to that of the 5-column Varicol system. The optimization results show that more subintervals and columns in a Varicol setup indeed favor optimal performance, as the eluent required is less for the same separation task. It is also confirmed that increasing the number of columns has greater effect on the optimum process performance than does increasing the number of subintervals.

Conclusions

Continuous large-scale chromatographic separations using simulated moving bed (SMB) technology have received a great deal of interest in recent years, particularly in the area of chiral separations. The countercurrent movement of the solid is achieved by switching the inlet and outlet ports in unison at a fixed predetermined switching time. Recently, Ludemann-Hombourger et al. (2000) reported a new system, that is, the Varicol process, that is based on the nonsynchronous shift of the inlet and outlet ports. They reported a mathematical model, which well reproduces the experimental results for the chiral separation of the 1,2,3,4-tetrahydro-1-naphthol racemate for both the SMB and the Varicol process. Their study showed that the performance of the Varicol process can exceed the performance of SMB systems due to the flexibility offered by the former in choosing variable column switching sequences. In this work, we presented a systematic study of the optimal operation of the SMB and Varicol processes using as an illustrative example the model of Ludemann-Hombourger et al. (2000). The selection of the operating parameters, such as column configuration, switching time interval (in SMB) and sequence (in Varicol), and liquid flow rates in different sections, is not straightforward. In most cases, conflicting requirements and constraints govern the optimal choice of the decision variables. In addition, the SMB and Varicol processes operate at high feed concentrations, leading to nonlinear competitive adsorption behaviors.

Table 7. Role of the Number of Columns and Subintervals on the Performance of an Optimized Varicol Process

Objective Function	Constraints		Decision Variables		Fixed Parameters	
Min E	$PurE = 0.95 \pm 0.002$ $PurE = x \pm 0.002$ $x = 0.95$ or 0.99		$18 < Q_2 < 27$ mL/min $4 < E < 6$ mL/min $0.5 < t_s < 1.0$ min χ (see Table 3)		$N_{col} = 5$ or 6 $F = 1.8$ or 1.05 mL/min $Q_1 = 27.5$ mL/min $V_{CSP} = 3.93 \times 10^{-5}$ m^3	
Optimum Solution						
Varicol Process	4-Subinterval, 5-Column		5-Subinterval, 5-Column		4-Subinterval, 6-Column	
PurR, %	95.02	98.86	94.89	98.81	94.80	98.85
PurE, %	94.94	98.86	94.93	98.80	94.99	99.00
F, mL/min	1.8	1.05	1.8	1.05	1.8	1.05
E, mL/min	*5.275*	*5.700*	*5.140*	*5.650*	*4.862*	*5.225*
Q_2, mL/min	*22.593*	*22.886*	*22.773*	*23.041*	*23.000*	*23.198*
t_s, min	*0.783*	*0.817*	*0.779*	*0.813*	*0.773*	*0.806*
χ	*D-C-C-B*	*D-C-C-B*	*D-C-C-B-A*	*D-C-C-B-A*	*A-A-C-E*	*A-B-C-E*

Note: Numbers in *shaded cell* are the optimum values.

The economical operation of the SMB (and Varicol) processes is governed by many factors depending on capital and operation costs, productivity, and product quality. One may be interested in higher productivity using minimum solvent (eluent), or may be interested in achieving as high purity as possible for the raffinate and extract product streams. In this work, we have considered two typical multiobjective optimization problems of interest in applications, which involve simultaneous optimization of more than one objective function. These included two cases: the simultaneous maximization of the purity of the raffinate and extract streams, and the maximization of the productivity with simultaneous minimization of eluent consumption. The optimization is done using a very robust, nondominated sorting genetic algorithm (NSGA). An optimal Pareto curve, which provides a set of optimal solutions that are equally good, is obtained for both the SMB and Varicol systems. It was found that the performance of a Varicol process is superior to that of a SMB process in terms of treating more feed using less eluent or producing better product quality for fixed productivity and solvent consumption. It is to be emphasized that there is no end to the variety of multiobjective optimization problems that can be formulated and studied, and we presented a few simple examples here to illustrate the concepts, techniques, and interpretation of our results. For the latter it has been shown that the concepts of the so-called triangle theory, based on the equilibrium theory of chromatography, are useful in rationalizing the results of this complex optimization problem.

Acknowledgments

We are grateful to Bayer AG for the financial support of this project. The help of S. Abel in constructing Figure 4 is gratefully acknowledged. One of the authors (AKR) acknowledges Professor S. K. Gupta of the Indian Institute of Technology, Kanpur, who introduced the exciting field of multiobjective optimization using genetic algorithm while he was visiting the National University of Singapore in 1999.

Notation

A = strongly adsorbed component
B = weakly adsorbed component
C = concentration, g/L
CSP = chiral stationary phase
E = eluent flow rate, mL/min
Ex = flow rate of extract stream, mL/min
F = feed flow rate, mL/min
H = column efficiency
I = objective function
J = theoretical number of cells, objective function
L = length of each column, m
m = flow-rate ratio parameter
N = number of columns
$PurE$ = purity of extract stream, %
$PurR$ = purity of raffinate stream, %
Q = fluid flow rate, mL/min
Ra = flow rate of raffinate stream, mL/min
SMB = simulated moving bed
t = time, min
u = velocity, m/s
V = volume, mL
Varicol = variable column system

Greek letters

χ = column configuration
ΔP = pressure drop
ϵ = bed porosity
ϕ = section numbers in SMB and Varicol

Subscripts and superscripts

col = column
f = feed
i = component i
j = section j
k = kth mixing cell
N = Nth switching period
M = Mth subinterval in Varicol
prev = previous
s = switching

Literature Cited

Bhaskar, V., S. K. Gupta, and A. K. Ray, "Applications of Multi-Objective Optimization in Chemical Engineering," *Rev. Chem. Eng.*, **16**, 1 (2000a).

Bhaskar, V., S. K. Gupta, and A. K. Ray, "Multiobjective Optimization of an Industrial Wiped Film Poly(ethylene terephthalate) Reactor," *AIChE J.*, **46**, 1046 (2000b).

Bhaskar, V., S. K. Gupta, and A. K. Ray, "Multiobjective Optimization of an Industrial Wiped Film Poly(ethylene terephthalate) Reactor: Some Further Insights," *Comput. Chem. Eng.*, **25**, 391 (2001).

Chankong, V., and Y. Y. Haimes, *Multiobjective Decision Making: Theory and Methodology*, Elsevier, New York (1983).

Charton, F., and R. M. Nicoud, "Complete Design of a Simulated Moving Bed," *J. Chromatogr. A*, **702**, 97 (1995).

Deb, K., *Optimization for Engineering Design: Algorithms and Examples*, Prentice Hall of India, New Delhi (1995).

Deb, K., "Evolutionary Algorithms for Multi-Criterion Optimization in Engineering Design," *Evolutionary Algorithms in Engineering and Computer Science: Recent Advances in Genetic Algorithms, Evolution Strategies, Evolutionary Programming, Genetic Programming and Industrial Applications*, K. Miettinen, P. Neittaanmäki, M. M. Mäkelä, and J. Périaux, eds., Wiley, New York (1999).

Deb, K., *Multi-Objective Optimization Using Evolutionary Algorithms*, Wiley, New York (2001).

Dunnebier, G., and K. U. Klatt, "Optimal Operation of Simulated Moving Bed Chromatographic Processes," *Comput. Chem. Eng.*, **23**, S195 (1999).

Fleming, P. J., "Applications of Multiobjective Optimization to Compensator Design for SISO Control Systems," *Electron. Lett.*, **22**, 258 (1986).

Fonseca, C. M., and P. J. Fleming, "Multiobjective Optimization and Multiple Constraint Handling with Evolutionary Algorithms: A Unified Formulation," *IEEE Trans. Syst., Man., Cybern.*, **A28**, 26 (1998).

Gentilini, A., C. Migliorini, M. Mazzotti, and M. Morbidelli, "Optimal Operation of Simulated Moving Bed Units for Non-Linear Chromatographic Separations: II. Bi-Langmuir Isotherm," *J. Chromatogr. A*, **805**, 37 (1998).

Goicoechea, A., D. R. Hansen, and L. Duckstein, *Multiobjective Decision Analysis with Engineering and Business Applications*, Wiley, New York (1982).

Goldberg, D. E., *Genetic Algorithms in Search, Optimization, and Machine Learning*, Addison-Wesley, Reading, MA (1989).

Holland, J. H., *Adaptation in Natural and Artificial Systems: An Introductory Analysis with Applications to Biology, Control and Artificial Intelligence*, Univ. of Michigan Press, Ann Arbor (1975).

Hollingdale, S. H., *Methods of Operational Analysis in Newer Uses of Mathematics*, J. Lighthill, ed., Penguin, New York (1978).

Juza, M., M. Mazzotti, and M. Morbidelli, "Simulated Moving Bed Chromatography and Its Application to Chirotechnology," *Trends Biotechnol.*, **18**, 108 (2000).

Karlsson, S., F. Pettersson, and T. Westerlund, "A MILP Method for Optimizing a Preparative Simulated Moving Bed Chromatographic Separation Process," *Comput. Chem. Eng.*, **23**, S487 (1999).

Ludemann-Hombourger, O., R. M. Nicoud, and M. Bailly, "The Varicol Process: A New Multicolumn Continuous Chromatographic Process," *Sep. Sci. Technol.*, **35**, 1829 (2000).

Mazzotti, M., G. Storti, and M. Morbidelli, "Robust Design of Countercurrent Adsorption Separation Processes 2. Multicomponent Systems," *AIChE J.*, **40**, 1825 (1994).
Mazzotti, M., G. Storti, and M. Morbidelli, "Robust Design of Countercurrent Adsorption Separation 3. Nonstoichiometric Systems," *AIChE J.*, **42**, 2784 (1996).
Mazzotti, M., G. Storti, and M. Morbidelli, "Robust Design of Countercurrent Adsorption Separation Processes 4. Desorbent in the Feed," *AIChE J.*, **43**, 64 (1997).
Migliorini, C., A. Gentillini, M. Mazzotti, and M. Morbidelli, "Design of Simulated Moving Bed Units Under Non-Ideal Conditions," *Ind. Eng. Chem. Res.*, **38**, 2400 (1999).
Mitra, K., K. Deb, and S. K. Gupta, "Multiobjective Dynamic Optimization of an Industrial Nylon 6 Semibatch Reactor using Genetic Algorithm," *J. Appl. Poly. Sci.*, **69**, 69 (1998).
Rajesh, J. K., S. K. Gupta, G. P. Rangaiah, and A. K. Ray, "Multiobjective Optimization of Steam Reformer Performance Using Genetic Algorithm," *Ind. Eng. Chem. Res.*, **39**, 706 (2000).
Rajesh, J. K., S. K. Gupta, G. P. Rangaiah, and A. K. Ray, "Multi-Objective Optimization of Industrial Hydrogen Plants," *Chem. Eng. Sci.*, **56**(3), 999 (2001).
Ravi, G., S. K. Gupta, and M. B. Ray, "Multiobjective Optimization of Cyclone Separators," *Ind. Eng. Chem. Res.*, **39**, 4272 (2000).
Rekoske, J. E., "Chiral Separations," *AIChE J.*, **47**, 2 (2001).
Ruthven, D. M., and C. B. Ching, "Countercurrent and Simulated Countercurrent Adsorption Separation Processes," *Chem. Eng. Sci.*, **44**, 1011 (1989).
Srinivas, N., and Deb, K., "Multiobjective Optimization Using Non-Dominated Sorting in Genetic Algorithms," *Evol. Comput.*, **2**, 106 (1995).
Storti, G., M. Masi, R. Paludetto, M. Morbidelli, and S. Carra, "Adsorption Separation Processes: Countercurrent and Simulated Countercurrent Operations," *Comput. Chem. Eng.*, **12**, 475 (1988).
Storti, G., M. Mazzotti, M. Morbidelli, and S. Carra, "Robust Design of Binary Countercurrent Adsorption Separation Processes," *AIChE J.*, **39**, 471 (1993).
Storti, G., R. Baciocchi, M. Mazzotti, and M. Morbidelli, "Design of Optimal Operating Conditions of Simulated Moving Bed Adsorptive Separation Units," *Ind. Eng. Chem. Res.*, **34**, 288 (1995).
Strube, J., A. Jupke, A. Epping, H. Schmidt-Traub, M. Schulte, and R. Devant, "Design, Optimization and Operation of SMB Chromatography in the Production of Enatiomerically Pure Pharmaceuticals," *Chirality*, **11**, 440 (1999).
Wu, D. J., Z. Ma, and N. H. L. Wang, "Optimization of Throughput and Desorbent Consumption in Simulated Moving Bed Chromatography for Paclitaxel Purification," *J. Chromatog. A*, **855**, 71 (1999).
Yuen, C. C., Aatmeeyata, S. K. Gupta, and A. K. Ray, "Multi-Objective Optimization of Membrane Separation Modules Using Genetic Algorithm," *J. Memb. Sci.*, **176**(2), 177 (2000).
Zhang, Z., K. Hidajat, and A. K. Ray, "Multiobjective Optimization of Simulated Countercurrent Moving Bed Chromatographic Reactor for MTBE Synthesis," *Ind. Eng. Chem. Res.*, **41**, 3213 (2002).
Zhou, F., S. K. Gupta, and A. K. Ray, "Multiobjective Optimization of the Continuous Casting Process for Poly(methyl methacrylate) Using Adapted Genetic Algorithm," *J. Appl. Poly. Sci.*, **78**, 1439 (2000).

Appendix: A Note on Genetic Algorithm (Srinivas and Deb, 1995; Deb, 2001)

The GA is a search technique developed by Holland (1978) that mimics the process of natural selection and natural genetics. In this algorithm, a set of decision variables is first coded in the form of a set of randomly generated binary numbers (0 and 1), called *strings* or *chromosomes*, thereby creating a "population (gene pool)" of such binary strings. Each chromosome is then mapped into a set of *real* values of the decision variables, using the upper and lower bounds of each of these. A model of the process is then used to provide values of the objective function for each chromosome. The value of the objective function of any chromosome reflects its "fitness." The Darwinian principle of "survival of the fittest" is used to generate a new and improved gene pool (new generation). This is done by preparing a "mating pool" that comprises copies of chromosomes, the number of copies of any chromosome being proportional to its fitness (Darwin's principle). Pairs of chromosomes are then selected randomly, and pairs of daughter chromosomes generated using operations similar to those in genetic reproduction. The gene pool evolves, with fitness improving over the generations.

Three common operators are used in GA [called simple GA (SGA), to distinguish it from its various adaptations] to obtain an improved (next) generation of chromosomes. These are referred to as reproduction, crossover, and mutation. Reproduction is the generation of the mating pool, where the chromosomes are copied probabilistically, based on their fitness values. However, no new strings are formed in the reproduction phase. *New* strings are created using the crossover operator by exchanging information among pairs of strings in the mating pool. A pair of daughter chromosomes is produced by selecting a crossover site (chosen randomly) and exchanging the two parts of the pair of parent chromosomes (selected randomly from the mating pool). The effect of crossover can be detrimental or beneficial. It is hoped that the daughter strings are superior. If they are worse than the parent chromosomes, they will slowly die a natural death over the next few generations (the Darwinian principle at work). In order to preserve some of the good strings that are already present in the mating pool, not all strings in the pool are used in crossover. A crossover probability, P_{cross}, is used, where only $100P_{\text{cross}}\%$ of the strings in the mating pool are involved in crossover, while the rest continue unchanged to the next generation. After a crossover is performed, mutation takes place. The mutation operator changes a binary number at *any* location in a chromosome from a 1 to a 0 and vice versa, with a small probability, P_{mute}. Mutation is needed to create a point in the neighborhood of the current point, thereby achieving a local search around the current solution and to maintain diversity in the population. The entire process is repeated until some termination criterion is met (the specified maximum number of generations is attained, or the improvements in the values of the objective functions become lower than a specified tolerance).

The optimal solutions to a multiobjective function optimization problem are nondominated (or optimal Pareto) solutions. In order to handle multiple objective functions and find optimal Pareto solutions, the SGA has been modified. The new algorithm, nondominated sorting genetic algorithm (NSGA), differs from the SGA only in the way the selection operator works.

The NSGA uses a ranking selection method to emphasize the good points and a niche method to create diversity in the population without losing a stable subpopulation of good points. In the new procedure, several groups of nondominated chromosomes from among all the members of the population at any generation are identified and classified into "fronts." Each of the members in a particular front is assigned a large, common, front fitness value (a dummy value) arbitrarily. To evenly distribute the points in this (or any other) front evenly in the variable decision domain, the dummy fitness value is then modified according to a sharing procedure by dividing it by the niche count of the chromosome. The niche count is a quantity that represents the num-

ber of neighbors around it, with distant neighbors contributing less than those nearby. The niche count, thus, gives an idea of how crowded the chromosomes are in the variable decision space. Using the shared fitness value for reproduction, thus, helps spread the chromosomes in the front, since crowded chromosomes are assigned lower fitness values. This procedure is repeated for all members of the first front. Once this is done, these chromosomes are temporarily removed from consideration, and all the *remaining* ones are tested for nondominance. The nondominated chromosomes in *this* round are classified into the next front. These are all assigned a dummy fitness value that is a bit lower than the *lowest* shared fitness value of the previous front. Sharing is performed thereafter. The sorting and sharing is continued until all the chromosomes in the gene pool are assigned shared fitness values. The usual operations of reproduction, crossover, and mutation are now performed. It is clear that the nondominated members of the first front with fewer neighbors will get the highest representation in the mating pool. Members of later fronts, which are dominated, will get lower representations (they are still assigned some low fitness values, rather than "killed," in order to maintain the diversity of the gene pool). Sharing forces the chromosomes to be spread out in the variable decision space. The population is found to converge very rapidly to the Pareto set. It should also noted that any number of objectives (both minimization and maximization problems) can be solved using this procedure. A flow chart describing this technique is presented below.

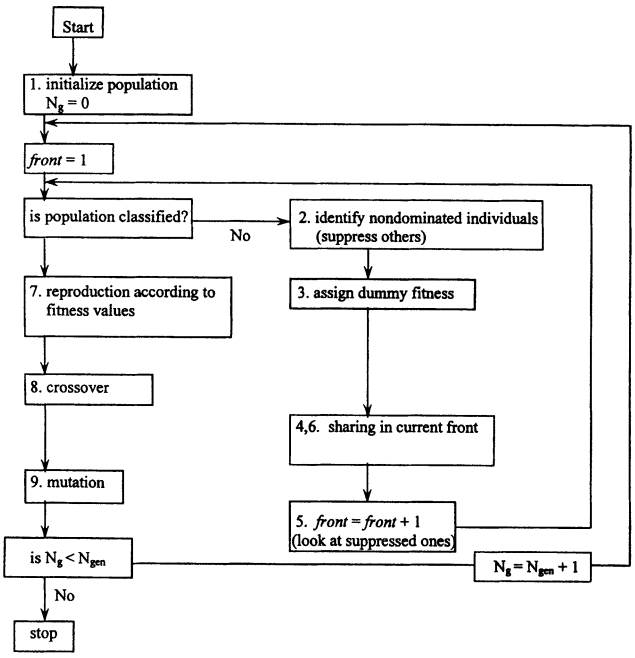

Scheme 1

Manuscript received Nov 12, 2001, and revision received May 29, 2002.